Dynamical Behavior of the H_2 Molecule of the $PtH(H_2)[P(t\text{-}Bu)_3]_2^+$ Complex. A Theory of Chemical Reactivity

Toshiaki Matsubara*

Center for Quantum Life Sciences and Graduate School of Science, Hiroshima University, 1-3-1, Kagamiyama, Higashi-Hiroshima 739-8530, Japan

Received: November 25, 2008; Revised Manuscript Received: January 2, 2009

The dynamical behavior of the coordinated H_2 molecule of the $PtH(H_2)[P(t\text{-}Bu)_3]_2]^+$ complex is examined by the ONIOM-molecular dynamics (MD) method that we recently developed. The ONIOM-MD simulations reveal that the dynamical environmental effects of the t-Bu substituents of the phosphine ligands, which increase the magnitude of the energy fluctuations of the active part, significantly promote both rotation and dissociation of the coordinated H_2 molecule. The Matsubara-RRK (M-RRK) theory proposed in this study and Matsubara's equation verify that the dynamical environmental effects are crucial factors to determine the chemical reactivity.

1. Introduction

The hybrid ONIOM method we developed[1−7] has overcome the restriction of the computational time, which has been one of serious problems of the quantum chemical calculation for a long time, and has made the quantum chemical calculation of the large molecular system possible. The computational algorithm of the ONIOM method is obviously different from the conventional QM/MM hybrid method. The calculation accuracy afforded for the model subsystem is maintained even for the real system by a simple extrapolation procedure.[5] The ONIOM method is now implemented in the GAUSSIAN03 program package[8] used all over the world, and is applied in a wide range of scientific fields, including nanomaterials, biomolecules and so on.[7]

However, we cannot apply the ONIOM method, which does not take account of the thermal motion of the nuclei, as it is, to the biomolecules such as enzymes in which the thermal fluctuations of the entire molecule would be closely related to their functions. On the other hand, the traditional molecular dynamics method based on the classical mechanics, which has been used so far, for example, for large-scale molecular dynamics simulations of proteins, describes well the dynamic behavior of the molecule due to the thermal motion of the nuclei, but not the electron rearrangement of the active part caused by a strong interaction or a reaction. The ONIOM-molecular dynamics (MD) method that we recently developed[9] successfully solved this dilemma. The ONIOM-MD method, integrating the ONIOM and MD methods, is a new hybrid quantum molecular dynamics method, which allows us to simulate the reaction in large molecular systems taking account of the effects of the thermal motion of the nuclei. Here, the concept embodied in the ONIOM method is retained intact. In the ONIOM-MD method, the direct MD simulations are performed calculating the energy and its gradient by the ONIOM method on the fly.

We have applied the ONIOM-MD method to cytidine and cytosine deaminase,[9−11] which are known as enzymes playing a key role in the activation of anticancer drugs inside the human body, and have succeeded in a quantum molecular dynamics simulation of the deamination reaction at the active site of the realistic model of enzyme in the solvent water. The contribution of the thermal motion of the environment to the reaction is now one of subjects of interest. We therefore especially focus on the effect of the amino acid residues environment on the substrate trapped in the pocket of the active site, which has not been paid attention to up to date.

As can be easily imaged, it has been general consensus that the trapped substrate in the pocket of the active site becomes unstable in energy. However, this fact was never proven and was a mere conjecture. The ONIOM-MD simulations have verified that the surrounding amino acid residues made the substrate trapped in the active site unstable in energy through their thermal motion.[9,11] The thermal motion of the neighboring amino acid residues environment perturbs the fluctuations in the geometry and energy of the substrate through the steric contact. We have also succeeded in specifying these amino acid residues. These effects are 'dynamical effects' of the environment, which is a new concept of the environmental effects we found. We have named these effects of the environment caused by the thermal fluctuations 'dynamical environmental effects'.[11]

The dynamical environmental effects are not special ones at the active site of enzymes. These effects would be also expected to play an important role in the active site of other systems surrounded by a similar environment. We have therefore applied the ONIOM-MD method to the prototype organometallic reaction, *cis*-$Pt(H)_2[P(t\text{-}Bu)_3]_2 \rightarrow H_2 + Pt[P(t\text{-}Bu)_3]_2$, to examine in detail the dynamical effects of the environment on the chemical reaction.[12]

The activation energy to evaluate the reactivity has been obtained from the energy profile of the entire molecule. However, the accurate activation energy of the reaction cannot be obtained by such a conventional manner, because the energy change in the environment, which is independent from the reaction, is also included in the energy profile. In the case of the reductive elimination of the H_2 from *cis*-$Pt(H)_2[P(t\text{-}Bu)_3]_2$, the essential barrier exits in the active part *cis*-$(H)_2Pt(PH_3)_2$. When this active part overcomes an energy barrier, the reaction proceeds. Since the active part and the environment behave independently, the reduction of the steric energy should be separated from the energy barrier of the reaction. In fact, the

* To whom correspondence should be addressed. E-mail: matsu05@hiroshima-u.ac.jp.

10.1021/jp810336u CCC: $40.75
Published on Web 03/10/2009

ONIOM-MD simulations have showed that after the detachment of the H_2 molecule from the Pt, the large steric repulsion between two phosphine ligands is reduced by the increase in the ∠P−Pt−P angle along the downhill energy surface. We have to assess the reactivity not by the energy barrier of the entire system including the environment but by the energy barrier of only the active part. The energy surface of the entire molecule is different from that of the active part. This difference is expected to enlarge when the target molecule becomes larger.

Thus, the reactivity of the chemical reaction is not quantitatively evaluated in the previous manner. The division of the entire molecule into the active and environment parts is indispensable. The effects of the environment are then considered in the active part. The traditional environmental effects, which are so-called static effects, are reflected in the energy barrier of the active part. On the other hand, dynamical effects, which we recently discovered,[9−11] are reflected in the energy fluctuations of the active part. The energy fluctuations as well as the energy barrier are one of factors to determine the reactivity, as we have shown.[12] The height of the energy barrier calculated from the energy surface of the reaction is not sufficient information. The reactivity has to be evaluated by the energy fluctuations in addition to the energy barrier.

However, the Arrhenius' equation contains only the energy barrier as a factor to determine the rate constant. We therefore newly derived Matsubara's eq 1 on the basis of the Arrhenius' equation to obtain the rate constant from the two factors, the energy fluctuations σ_E^{QM} and the energy barrier ΔE^{QM}.[12]

$$k = A \exp\left(-\sqrt{\frac{f^{\mathrm{QM}}}{2}}\frac{\Delta E^{\mathrm{QM}}}{\sigma_E^{\mathrm{QM}}}\right) \quad (1)$$

Here, the energy fluctuations σ_E^{QM} in addition to the energy barrier ΔE^{QM} are connected to the rate constant k. f^{QM} is the number of degree of freedom of the active part. This equation tells us that the reaction becomes more facile when the dynamical environmental effects enlarge the energy fluctuations of the active part. In fact, it has been revealed that the energy fluctuations of the active part enlarged by the dynamical environmental effects due to the thermal motion of the bulky substituents t-Bu of the phosphine ligands facilitate the H_2 reductive elimination of the *cis*-$Pt(H)_2[P(t\text{-}Bu)_3]_2$ complex.[12] This corresponds to the fact that the active part is just embedded in a bath of the environment and heated by the thermal motion of the environment. The dynamical environmental effects thus dominantly contribute to the reactivity of the chemical reaction through the energy fluctuations.

Eq 1 also teaches us that the energy fluctuations are the energy source and driving force to overcome the energy barrier. We therefore readily notice that the energy fluctuations can be introduced to the RRK theory and thereby the dynamical environmental effects are evaluated through the energy fluctuations from a different aspect. In the present study, we improved the RRK theory and applied to the dynamical behavior of the $PtH(H_2)[P(t\text{-}Bu)_3]_2^+$ complex,[13] which is one of many H_2-coordinated transition metal complexes synthesized because of their versatile utilities for the organic syntheses.[14] We also applied Matsubara's equation and revealed that the dynamical environmental effects of the substituents t-Bu of the phosphine ligands are the crucial factors to determine the reactivity of the coordinated H_2 molecule.

2. Computational Details

We adopted three model complexes $PtH(H_2)(PR_3)_2^+$ (R = t-Bu, Me, and H) with the different substituents of the phosphine ligands to examine the environmental effects on the behavior of the coordinated H_2 molecule. We performed the QM and ONIOM calculations for R = H and R = t-Bu and Me, respectively. For the ONIOM calculations, two-layered ONIOM methodology, which divides the entire molecule into the inner and outer layers, was used. We included the active part $PtH(H_2)(P)_2^+$ in the inner layer and the Me and t-Bu substituents, which would affect the inner layer, in the outer layer. All the cut P−C bonds were capped with the H atoms to form a subsystem $PtH(H)_2(PH_3)_2^+$ of the inner layer.

The inner layer was treated by the quantum mechanical (QM) method at the Hartree−Fock (HF) level of theory. We used the basis set, referred to as BSI below, which consists of the relativistic effective core potential (ECP) replacing the core electrons up to 4f with the valence double ζ (8s,6p,3d)/[3s,3p,2d] basis functions by Hay-Wadt for Pt,[15] 6−311G** for H of the dihydrogen molecule and hydride, and the standard STO-2G for PH_3. The outer layer was treated by the molecular mechanics (MM) method using the MM3 force field parameters. The van der Waals parameters reported by Rappe et al. were used for the Pt atom.[16] The torsional contributions associated with dihedral angles involving Pt were set to zero. For the other atoms, the standard MM3 parameters were used. The ONIOM energy and gradients are expressed by the sum of the QM and MM energies and gradients of the inner and outer layers as follows.

$$E_{\mathrm{ONIOM,real}}(\mathbf{R}_{\mathrm{inner}},\mathbf{R}_{\mathrm{outer}}) = E_{\mathrm{QM,inner}}(\mathbf{R}_{\mathrm{inner}},\mathbf{R}_{\mathrm{link}}) + E_{\mathrm{MM,outer}}(\mathbf{R}_{\mathrm{outer}}) \quad (2)$$

$$E_{\mathrm{MM,outer}}(\mathbf{R}_{\mathrm{outer}}) = E_{\mathrm{MM,real}}(\mathbf{R}_{\mathrm{inner}},\mathbf{R}_{\mathrm{outer}}) - E_{\mathrm{MM,inner}}(\mathbf{R}_{\mathrm{inner}},\mathbf{R}_{\mathrm{link}}) \quad (3)$$

$$\partial E_{\mathrm{ONIOM,real}}/\partial \mathbf{R}_{\mathrm{real}} = (\partial E_{\mathrm{QM,inner}}/\partial \mathbf{R}_{\mathrm{inner}})\mathbf{J}(\mathbf{R}_{\mathrm{link}};\mathbf{R}_{\mathrm{inner}},\mathbf{R}_{\mathrm{outer}}) + \partial E_{\mathrm{MM,real}}/\partial \mathbf{R}_{\mathrm{real}} - (\partial E_{\mathrm{MM,inner}}/\partial \mathbf{R}_{\mathrm{inner}})\mathbf{J}(\mathbf{R}_{\mathrm{link}};\mathbf{R}_{\mathrm{inner}},\mathbf{R}_{\mathrm{outer}}) \quad (4)$$

All the QM- and ONIOM-molecular dynamics (MD) simulations were performed using the HONDO-2001 program.[17] In both QM- and ONIOM-MD methods, a direct MD simulation was performed calculating the QM or ONIOM energy and its gradients on the fly. The time evolution of the nuclei was performed with the Beeman algorithm.[18] The simulations were run under the constant temperature with a time step of 1 fs. A Berendsen thermostat[19] with a coupling constant of 100 fs was used to keep the temperature constant.

The data collected every 10 fs from 5 to 100 ps were used to calculate the average, standard deviation of the geometric parameters, energy, and force, unless otherwise noted, because the potential energy of the entire system as well as the temperature becomes almost constant after 5 ps. The standard deviation σ is defined as follows.

$$\sigma = \sqrt{\frac{1}{n}\sum_{i=1}^{n}(X_i - \bar{X})^2} \quad (5)$$

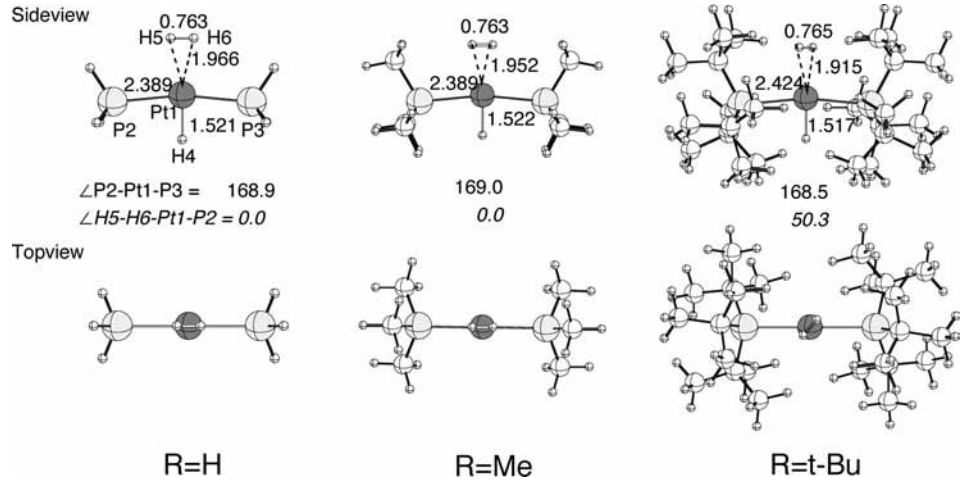

Figure 1. Optimized structures (Å, deg) of $Pt(H)(H_2)(PR_3)_2^+$ by the QM(HF/BSI) method for R = H and by the ONIOM(HF/BSI:MM3)-MD method for R = Me and t-Bu.

The geometry optimizations for R = Me and t-Bu were performed by the ONIOM-MD method by solving Newton's equations of motion at zero Kelvin. The nuclei with the initial velocities of zero start to move on the potential energy surface downward. The velocities generated during movement along the potential energy surface are always maintained extremely small by the velocity scaling of the Berendsen thermostat set to zero. The nuclei slowly come close to the minimum of the potential energy surface and finally stop at the minimum with the velocities of zero.

On the other hand, the geometry optimizations and the energy calculations for R = H were carried out by using the GAUSSIAN03 program.[8] In addition to the HF level, the B3LYP level of density functional theory, which consists of a hybrid Becke + Hartree−Fock exchange and a Lee−Yang−Parr correlation functional with nonlocal corrections,[20,21] was also used with the basis set BSII, where LANL2DZ instead of STO-2G is used for PH_3.

The binding energy (BE) of the H_2 with the $PtH(PH_3)_2^+$ fragment was calculated as a sum of the interaction energy (INT) and deformation energy (DEF) as follows.

$$\mathrm{BE} = \mathrm{INT} + \mathrm{DEF} \tag{6}$$

The INT and DEF energies are defined as,

$$\mathrm{INT} = E[\mathrm{H_2}](\mathrm{d}) + E[\mathrm{PtH(PR_3)_2^+}](\mathrm{d}) - E[\mathrm{PtH(H_2)(PR_3)_2^+}] \tag{7}$$

$$\mathrm{DEF} = E[\mathrm{H_2}] - E[\mathrm{H_2}](\mathrm{d}) + E[\mathrm{PtH(PR_3)_2^+}] - E[\mathrm{PtH(PR_3)_2^+}](\mathrm{d}) \tag{8}$$

Here, E(d) means the energy required to deform the structure for the interaction.

3. Results and Discussion

3.1. Optimized Structures and Binding and Rotational Energies of the H_2 Molecule of the $PtH(H)_2(PR_3)_2^+$ (R = H, Me, and t-Bu) Complexes. The optimized structures of $PtH(H)_2(PR_3)_2^+$ (R = H, Me, and t-Bu) are presented in Figure 1. The H_2 molecule is weakly bound at the Pt, and its H−H distance is hardly stretched compared to that of the free H_2 molecule. This is consistent with the previous computational results.[13] This weak coordination of the H_2 molecule is understood by the charge transfer interactions between the H_2 and the $PtH(PR_3)_2^+$ fragment displayed in Scheme 1. The electron donation from the H_2 σ orbital to the vacant dspσ orbital of the Pt strongly occurs because of the existence of the H^+ ligand in trans. On the other hand, the electron back-donation from the occupied dπ orbital of the Pt to the H_2 σ^* orbital is weak because the dπ orbital of the Pt is not destabilized in energy to easily interact with H_2 σ^* orbital due to the large P−Pt−P angle of around 170°.

SCHEME 1

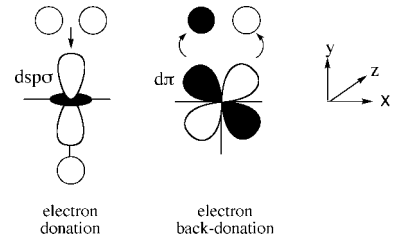

It is obvious that the environmental effects of the substituents of the ligands affect some geometric parameters of the inner part. The loosely bound H_2 is drawn toward to the Pt by the steric effect of the congested t-Bu as shown by the Pt1−H6 distance shortened to 1.915 Å. The Pt1−H4 distance is also slightly shortened. The bulky substituent t-Bu restricts the space of the inner part, and then the coordinated H_2 and hydrido ligands are confined in a smaller space. The Pt1−H6 distance decreases according to the order in the bulkiness of the substituents, H > Me > t-Bu. On the other hand, the Pt−P distances are lengthened by 0.035 Å in the case of R = t-Bu compared to the case of R = H, while there is no significant difference in the angle ∠P2−Pt1−P3 among R = H, Me, and t-Bu.

The t-Bu environment also affects the orientation of the coordinated H_2 molecule. Although the H_2 axis is parallel to the P2−Pt1−P3 axis in the case of R = H and Me, it deviates from the P2−Pt1−P3 axis by 50.3° in the case of R = t-Bu as shown by the dihedral angle ∠H5−H6−Pt1−P2. In the case of R = H, the basis set also affects the orientation of the coordinated H_2 (Table 1).

The rotation energies of the H_2 molecule for R = H at the HF/BSI and B3LYP/BSII levels are similar. These small rotation energies of around 1 kcal/mol are in good agreement with the

TABLE 1: Interaction (INT), Binding (BE), and Rotation Energies (kcal/mol) of the H_2 of $PtH(H_2)(PH_3)_2^+$ at Various Levels

level	orientation of the H_2[a]	INT	BE[b]	rotation energy
HF/BSI	parallel	10.2	8.9	0.8
HF/BSII	perpendicular	7.0	6.3	0.5
B3LYP/BSII	perpendicular	12.8	11.1	1.2

[a] The orientation of the H_2 axis on the P−Pt−P axis. [b] BE = INT + DEF. See the text for the details.

TABLE 2: Interaction (INT) and Binding (BE) Energies (kcal/mol) of the H_2 of $PtH(H_2)(PR_3)_2^+$ (R = Me and t-Bu) at the ONIOM(HF/BSI:MM3) Level

	INT		BE[a]	
R	QM energy	ONIOM energy	QM energy	ONIOM energy
Me	9.7	10.0	8.4	8.7
t-Bu	8.9	7.1	9.0	1.8

[a] BE = INT + DEF. See the text for the details.

experimental values of 0.5−2.0 kcal/mol reported for the other complexes.[22] On the other hand, the INT is a little larger at the B3LYP/BSII level than at the HF/BSI level. Since the HF/BSI level thus gives good results, we adopted the HF/BSI level for the molecular dynamics (MD) simulations saving the computational time. The binding energy (BE) is smaller only by 1−2 kcal/mol than the INT in each level, which indicates that the deformation energy (DEF) of the H_2 and $PtH(PR_3)_2^+$ required for the interaction between them is very small.

Both INT of 10.0 kcal/mol and BE of 8.7 kcal/mol of the coordinated H_2 molecule in the ONIOM energy for R = Me (Table 2) are nearly the same as those for R = H. On the other hand, the INT in the ONIOM energy for R = t-Bu is reduced to 7.1 kcal/mol because of the steric effect of the t-Bu substituents. This value is similar to the activation energy of 11 kcal/mol experimentally reported for the H_2 dissociation of the $PtH(H)_2[P(t\text{-}Bu)_3]_2^+$ complex.[13] It should be noted that in the ONIOM energy for R = t-Bu the BE of 1.8 kcal/mol is much smaller compared to the INT of 7.1 kcal/mol because the DEF is large in the case of the sterically congested t-Bu. The DEF is much larger for the outer layer than for the inner layer, as shown by the fact that both INT and BE are nearly the same in the QM energy of the inner layer.

3.2. QM- and ONIOM-Molecular Dynamics (MD) simulations of $PtH(H)_2(PR_3)_2^+$ (R = H, Me, and t-Bu). The molecular dynamics (MD) simulations of $PtH(H)_2(PR_3)_2^+$ (R = H, Me, and t-Bu) were performed at 200 K, since the behavior of the coordinated H_2 of $PtH(H)_2[P(t\text{-}Bu)_3]_2^+$ has been examined at around this temperature in experiment.[13] The average and the standard deviation of the selected geometric parameters in the MD simulations of $PtH(H)_2(PR_3)_2^+$ (R = H, Me, and t-Bu) are presented in Table 3. We can find some tendencies in the bond distances among the substituents R, although there is no significant difference in the P2−Pt1−P3 angle. The average of the Pt1−P2 distance becomes large in the order t-Bu > Me > H with the increase in the steric effect of the substituent. The steric effect of the substituents is more obviously reflected in the Pt1−H4 and Pt1−H5 distances. The averages of the Pt1−H4 and Pt1−H5 distances are the smallest for R = t-Bu, since both hydride and coordinated H_2 are confined in the restricted space of the inner layer by the sterically congested t-Bu substituents, as mentioned earlier. However, the average of the Pt1−H5 distance is stretched by 0.040 Å compared to the optimized one even for R = t-Bu because the weak interaction of the H_2 with Pt is strongly affected by the thermal motion. On the other hand, the average of the Pt1−P2 distance is the largest for R = t-Bu. The standard deviation for the Pt−H4, Pt1−H5, and Pt1−P2 distances is also large for R = t-Bu because the vibration of these bonds is strongly perturbed by the thermal motion of the bulky t-Bu. To the contrary, the distance of the rigid H5−H6 bond is hardly affected by the thermal motion even for R = t-Bu, as shown by the small standard deviation and the average similar to the optimized one.

It has been one of issues whether the oxidative addition and reductive elimination of the coordinated H_2 occurs as follows, which is not clearly proven in experiment yet.

$$Pt^{II}H(H_2)[P(t\text{-}Bu)_3]_2^+ \rightleftharpoons Pt^{IV}(H)_3[P(t\text{-}Bu)_3]_2^+ \quad (9)$$

To get an answer to this question, we examined the maximum and minimum of the Pt−H_2 and H−H distances in the MD simulations at 200 K (Table 4). Two H of the coordinated H_2 behave similarly on the Pt atom so that the Pt1−H5 and Pt1−H6 distances change in the same manner. In the case of R = t-Bu, both Pt1−H5 and Pt1−H6 distances are shortened to 1.68 Å, which are similar to those for the normal hydrides. Nevertheless, the H5−H6 distance is always less than 1.0 Å. These results show that the oxidative addition of the H_2 does not take place. The weak electron back-donation from an occupied dπ orbital of the Pt to the H_2 σ^* orbital mentioned earlier would not allow the complete H−H cleavage. On the other hand, the Pt1−H5 and Pt1−H6 distances are stretched up to 2.62 Å, although the H_2 does not go away from the Pt completely. This would support the experimental result that the coordination and dissociation of the H_2 is reversible.[13]

$$Pt^{II}H(H_2)[P(t\text{-}Bu)_3]_2^+ \rightleftharpoons Pt^{II}H[P(t\text{-}Bu)_3]_2^+ + H_2 \quad (10)$$

3.3. Rotation of the H_2 Molecule on the Pt of $PtH(H)_2(PR_3)_2^+$ (R = H, Me, and t-Bu). The rotation of the coordinated H_2 molecule on the Pt was observed for the $PtH(H_2)[P(t\text{-}Bu)_3]_2^+$ complex in the MD simulations at 200 K. Although this H_2 rotation of the $PtH(H_2)[P(t\text{-}Bu)_3]_2^+$ complex has not been experimentally confirmed, the same H_2 rotation has been experimentally reported for other H_2-coordinated complexes.[23] The change in the dihedral angle ∠H5−H6−Pt1−P2 for R = H, Me, and t-Bu are presented in Figure 2. The magnitude of the dihedral angle ∠H5−H6−Pt1−P2 remarkably oscillates in the case of R = t-Bu, which shows that the coordinated H_2 rotates again and again. The number of times of H_2 rotation is much reduced in the case of R = Me, although the H_2 still rotates frequently. On the other hand, the H_2 hardly rotates in the case of R = H. The other simulations for R = H showed no rotation of the H_2 during 100 ps (Figure S1, Supporting Information). This difference in the rotation of the H_2 is reflected in the ratio of the dihedral angle ∠H5−H6−Pt1−P2 as presented in Table 5. The ratio of the dihedral angle ∠H5−H6−Pt1−P2, being more than 150° and less than 30°, is obviously small for R = t-Bu, because the H_2 axis largely deviates from the P2−Pt1−P3 axis for a long time because of its rotation. This ratio becomes larger for R = Me where number of times of H_2 rotation decreases.

The force added to the inner layer from the environment of the outer layer, which is important as a driving force of an action in the inner layer as reported previously,[12] was examined. The force added to the H_2 and hydride of the inner layer from the

TABLE 3: Average and Standard Deviation of the Selected Geometric Parameters (Å, deg) of $PtH(H_2)(PR_3)_2^+$ in the QM(HF/BSI)-MD (R = H) and ONIOM(HF/BSI:MM3)-MD (R = Me and t-Bu) Simulations at 200 K Together with Their Optimized Values[a]

	d(Pt1−H4)			*d*(Pt1−H5)			*d*(H5−H6)			*d*(Pt1−P2)			∠(P2−Pt1−P3)		
R	optimized	average	standard deviation	optimized	average	standard deviation	optimized	average	standard deviation	optimized	average	standard deviation	optimized	average	standard deviation
H	1.521	1.519	0.015	1.966	1.980	0.058	0.763	0.764	0.025	2.389	2.388	0.030	168.9	169.5	2.2
Me	1.522	1.520	0.027	1.952	1.999	0.091	0.763	0.763	0.021	2.389	2.395	0.033	169.0	169.5	2.8
t-Bu	1.517	1.513	0.028	1.915	1.955	0.092	0.765	0.764	0.021	2.424	2.430	0.036	168.5	168.7	2.7

[a] Data of runs 1 and 2 were used for R = H, Me, and R = t-Bu, respectively.

TABLE 4: Maximum and Minimum Values of the Selected Geometric Parameters (Å) of $PtH(H_2)(PR_3)_2^+$ in the QM(HF/BSI)-MD (R = H) and ONIOM(HF/BSI:MM3)-MD (R = Me and t-Bu) Simulations at 200 K

	d(Pt1−H4)		*d*(Pt1−H5)		*d*(Pt1−H6)		*d*(H5−H6)	
R	maximum	minimum	maximum	minimum	maximum	minimum	maximum	minimum
Run 1[a]								
H	1.558	1.486	2.210	1.809	2.214	1.793	0.822	0.713
Me	1.586	1.457	2.355	1.732	2.378	1.750	0.829	0.714
t-Bu								
Run 2								
H	1.556	1.483	2.266	1.800	2.232	1.785	0.815	0.717
Me	1.583	1.462	2.343	1.744	2.317	1.750	0.834	0.708
t-Bu	1.604	1.436	2.474	1.700	2.455	1.695	0.833	0.703
Run 3								
H	1.549	1.487	2.203	1.804	2.191	1.821	0.811	0.717
Me	1.592	1.454	2.426	1.732	2.442	1.747	0.832	0.703
t-Bu	1.586	1.438	2.615	1.678	2.617	1.679	0.835	0.712

[a] The results for R = t-Bu are not presented because the H_2 dissociated during the MD simulation.

TABLE 5: Ratio (%) of the Dihedral Angle ∠H5−H6−Pt1−P2 That Is More than 150° and Less than 30° in the QM(HF/BSI)-MD (R = H) and ONIOM(HF/BSI:MM3)-MD (R = Me and t-Bu) Simulations of $PtH(H_2)(PR_3)_2^+$ at 200 K

	run 1[a]			run 2			run 3		
R	>150°	<30°	total	>150°	<30°	total	>150°	<30°	total
H	0.1	79.0	79.1	0.1	69.2	69.3	0.0	83.0	83.0
Me	13.1	44.0	57.1	13.0	45.0	58.0	32.2	23.9	56.1
t-Bu				10.3	9.3	19.6	9.3	10.4	19.7

[a] The results for R = t-Bu are not presented because the H_2 dissociated during the MD simulation.

substituents R of the outer layer is presented in Figure 3. When R is t-Bu, the H_2 (H5, H6) of the inner layer feels a large force from the environment. It should be noted that a large force is also added to the hydride (H4). This would significantly affect the action of the H_2 through the trans influence. As shown in Figure 3B, as a matter of course, the force added to the H_2 (H5, H6) becomes zero after the H_2 disociates from the Pt at 41.9 ps. The force added to the hydride (H4) also becomes smaller after the H_2 dissociation because the entire molecule is sterically relaxed. In the case of less congested substituent of Me, these forces added to the H_2 (H5, H6) and hydride (H4) are quite small as shown in Figure 3C.

The forces added to the H4, H5, and H6 atoms from the substituents R was analyzed in more detail (Table 6). In the case of R = t-Bu, the average of the added force is about two times larger on the H4 than on the H5 and H6, although the

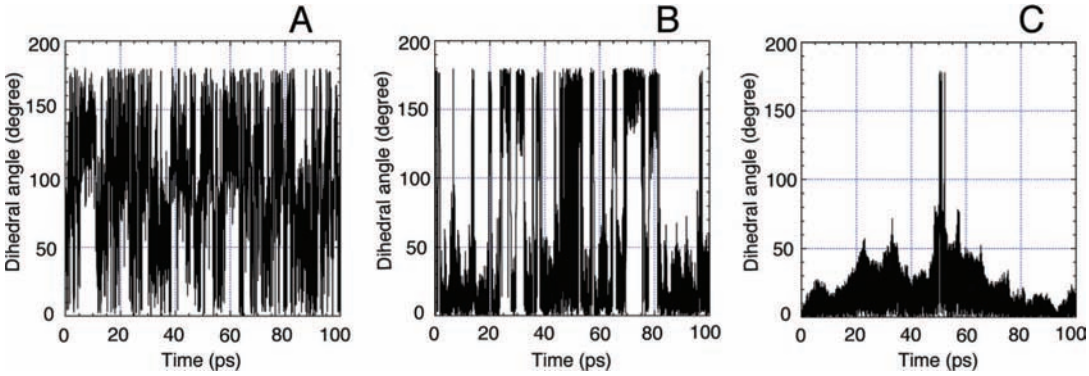

Figure 2. Changes in the dihedral angle ∠H5−H6−Pt1−P2 of $PtH(H_2)(PR_3)_2^+$ in the QM(HF/BSI)-MD simulation for R = H and ONIOM(HF/BSI:MM3)-MD simulations for R = Me and t-Bu at 200 K. A: R = t-Bu, B: R = Me, C: R = H.

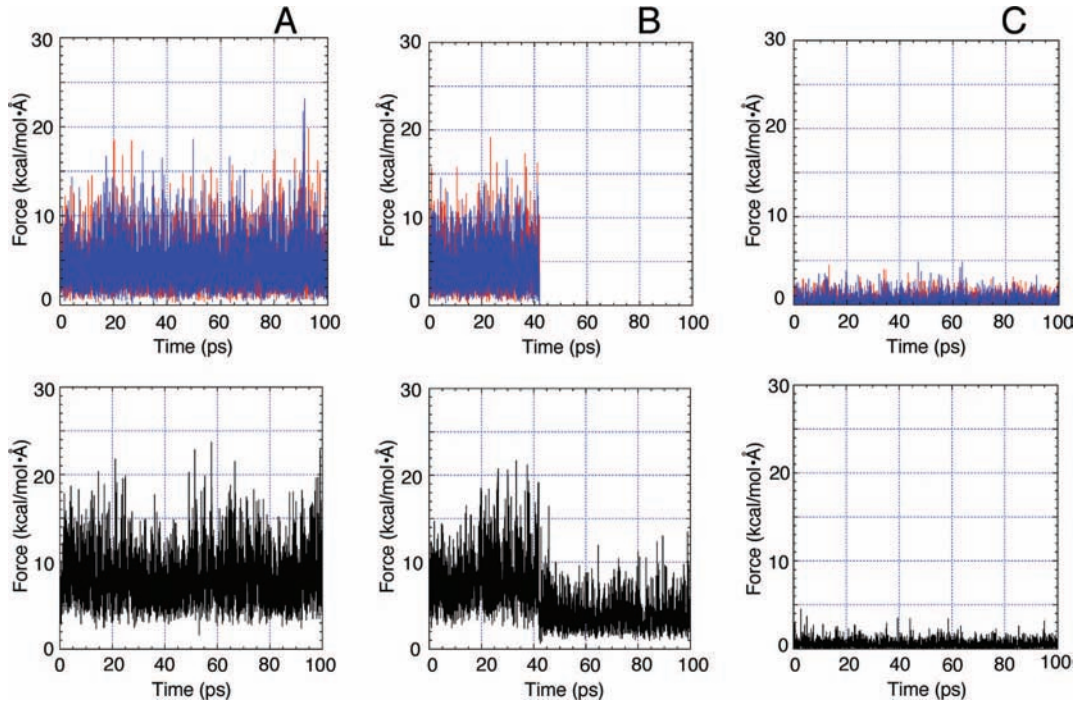

Figure 3. Changes in the forces added to the H4, H5, and H6 atoms of the inner layer from the substituents R of the outer layer in $PtH(H_2)(PR_3)_2^+$ (R = Me and t-Bu) during the ONIOM(HF/BSI:MM3)-MD simulations at 200 K. A: R = t-Bu, B: R = t-Bu with the H_2 dissociation at 41.9 ps, C: R = Me. In A, B, and C, red: H5, blue: H6, and black: H4.

TABLE 6: Average and Standard Deviation of the Forces (kcal/mol·Å) Added to the H4, H5, and H6 Atoms of the Inner Layer from the Substituents R of the Outer Layer and Number of Times Exceeding 5 and 10 kcal/mol·Å in the ONIOM(HF/BSI:MM3)-MD Simulations of $PtH(H_2)(PR_3)_2^+$ (R = Me and t-Bu) at 200 K

	H4				H5				H6			
R	average	standard deviation	>5	>10	average	standard deviation	>5	>10	average	standard deviation	>5	>10
Run 1[a]												
Me	0.448	0.332	0	0	0.463	0.444	0	0	0.468	0.453	0	0
t-Bu	7.804	2.641			4.304	2.386			4.330	2.369		
Run 2												
Me	0.478	0.368	0	0	0.459	0.453	2	0	0.451	0.433	1	0
t-Bu	7.789	2.676	8768	1910	4.372	2.384	3328	273	4.294	2.348	3128	255
Run 3												
Me	0.452	0.340	0	0	0.457	0.477	3	0	0.455	0.482	0	0
t-Bu	7.818	2.431	9023	1682	4.211	2.246	3025	200	4.221	2.286	3090	218

[a] For R = t-Bu, the data collected from 5 to 40 ps was used because the H_2 dissociated at 41.9 ps. The number of times that 5 and 10 kcal/mol·Å is exceeded is omitted.

standard deviation is similar among them. The number of times that 10 kcal/mol·Å is exceeded is also about eight times larger on the H4 than on the H5 and H6. These results suggest that the force on the H4 as well as those on the H5 and H6 is important as a driving force and significantly contributes to the action of the H_2 through the trans influence.

3.4. Dissociation of the H_2 from the Pt of $PtH(H)_2(PR_3)_2^+$ (R = H, Me, and t-Bu). In the case of R = t-Bu, the H_2 is eliminated from the Pt at 200 K during 100 ps in some trajectories, although not in the case of R = Me as far as we tried. The changes in the selected geometric parameters for a trajectory in the case of R = t-Bu where the H_2 is eliminated is presented in Figure 4. One can readily find a correlation between the vibration of the Pt−H4 bond and those of the Pt−H5 and H5−H6 bonds. When the oscillation of the Pt−H4 distance increases, the oscillation of both Pt−H5 and H5−H6 distances also increase. This would be understood by a trans influence of the hydride H4. For example, when the Pt−H4 bond is stretched, the electron donation from the H_2 σ orbital to an unoccupied dspσ orbital of the Pt is weakened so that the Pt−H_2 distance increases. The H4 is thus considered to function as an initiator of the H_2 dissociation. The thermal fluctuations of the H4 enlarged by the force from the environment mentioned earlier induce the H_2 dissociation. The Pt−H_2 interaction weakened by the motion of the H4 is finally broken by the force added to the H_2 from the environment. As we previously reported for the reaction, *cis*-$Pt(H)_2[P(t\text{-}Bu)_3]_2 \rightarrow H_2 + Pt[P(t\text{-}Bu)_3]_2$, the attack of some terminal H of the t-Bu to the Pt also enhances the vibration of the Pt−H_2 and promotes the H_2 dissociation (see Figure S2, Supporting Information). Without the sufficient motion of the H4, no H_2 dissociation occurs as shown in Figure S3, Supporting Information. For example, in run 3, the H_2 never dissociates, although the Pt−H_2 distance is stretched to more than 2.5 Å at 82.5 ps. The P2−Pt1−P3 angle increases after the H_2 dissociation because of the sterical relaxation of the entire molecule. This shows that an action of the H_2 is achieved when the inner layer overcomes its own energy barrier, as we

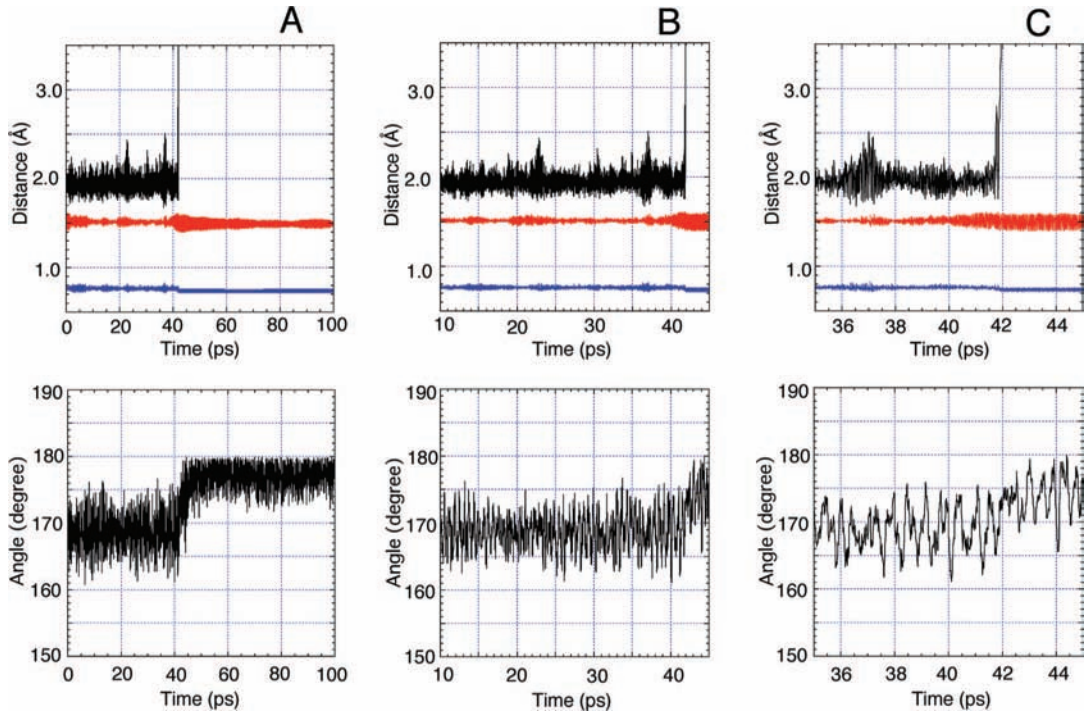

Figure 4. Changes in the selected geometric parameters in the reaction, $PtH(H_2)[P(t\text{-}Bu)_3]_2^+ \rightarrow H_2 + Pt(H)[P(t\text{-}Bu_3)_2]^+$, during the ONIOM(HF/BSI:MM3)-MD simulation at 200 K. Bond distances; black: d(Pt1−H5), red: d(Pt1−H4), blue: d(H5−H6). Bond angle; black: ∠P2−Pt1−P3. A, B, and C have different time scales.

previously reported.[12] The real energy barrier of the reaction exists in the inner layer of the active part.

When the temperature is increased to 250 K, the H_2 was readily released from the Pt (see Figure S4, Supporting Information). All the trajectories showed the detachment of the H_2 from the Pt in the initial stage of the MD simulations. Here, also an increase in the vibration of the Pt−H4 bond was found just before the H_2 dissociation.

As presented in Figures S5 and S6, Supporting Information, there exists no significant change in the oscillation of the Pt−H4 distance for both R = H and Me. This is due to the small dynamical environmental effects of the less bulky substituents. On the other hand, although the Pt−H_2 distance remarkably oscillates by the thermal motion even in the case of R = Me, which is similar to the case of R = t-Bu (see Table 3), the H_2 never dissociates without the support of the H4 (Figure S5). In the case of R = H, the thermal oscillation of the Pt−H_2 distance is also small (Figure S6), because the little force is added from the H environment.

When the temperature is increased to 300 K, the H_2 dissociates in some trajectories for R = Me (see Figure S7, Supporting Information). However, there is no longer distinct correlation between the oscillations of the Pt1−H4 and Pt1−H5 distances. It is thought that a sufficient energy required to eliminate the H_2 can be provided at 300 K and the support of the H4 is not necessary. For R = H, the H_2 still does not dissociate even at 300 K.

3.5. Evaluation of the Reactivity of the H_2 Rotation of $PtH(H)_2(PR_3)_2^+$ (R = H, Me, and t-Bu) by the Matsubara-RRK Theory. Now, the next subject to understand is how the actions of the H_2 molecule, the rotation and dissociation, mentioned earlier take place with the energy fluctuations. Although we have revealed that the energy fluctuations are the energy source and driving force of the chemical reaction by Matsubara's equation in the previous study,[12] we are just at the initial stage on the understanding how the reaction proceeds. In this section, we apply the concept of the energy fluctuations to the RRK theory, which is one of well-known theories of chemical reactions. Because the energy required to overcome a barrier is provided from the energy fluctuations,[12] this application would be quite reasonable.

Let us assume that a molecule A consists of oscillators s with the quanta j and all these oscillators s have a same frequency ν. The number of ways to distribute j quanta into s oscillators, ω_j, is written as follows.

$$\omega_j = \frac{(j + s - 1)!}{j!(s - 1)!} \tag{11}$$

On the other hand, in the case that m quanta out of j are distributed to one oscillator, the number of ways to distribute the remaining $j - m$ quanta into $s - 1$ oscillators is

$$\omega_{j,m} = \frac{(j - m + s - 1)!}{(j - m)!(s - 1)!} \tag{12}$$

Therefore, the probability that a particular oscillator contains at least m quanta for the reaction is expressed as

$$P = \frac{\omega_{j,m}}{\omega_j} = \frac{(j - m + s - 1)!j!}{(j - m)!(j + s - 1)!} \tag{13}$$

Here, if we use the Stirling's approximation $n! \approx (2\pi n)^{1/2}(n/e)^n$ $(n >> 0)$, eq 13 is written as follows,

$$P = \frac{(j - m + s - 1)^{j-m+s-1}j^j}{(j - m)^{j-m}(j + s - 1)^{j+s-1}} \tag{14}$$

If we assume $j - m \gg s - 1$, eq 14 is

$$P = \left(1 - \frac{m}{j}\right)^{s-1} \tag{15}$$

When the critical energy for the reaction is $\Delta E = mh\nu$, eq 15 is written with the total energy of $\varepsilon = jh\nu$ of the molecule A as

$$P = \left(1 - \frac{\Delta E}{\varepsilon}\right)^{s-1} \tag{16}$$

This is the probability of a reaction of the molecule A derived on the basis of the RRK theory. Here, the total energy ε of the molecule A should be replaced by the energy fluctuations as follows because the energy required to overcome the energy barrier is in fact provided from the energy fluctuations as mentioned earlier.

$$P = \left(1 - \frac{\Delta E^{\mathrm{QM}}}{2\sigma_E^{\mathrm{QM}}}\right)^{f^{\mathrm{QM}}-1} \tag{17}$$

Here, σ_E^{QM}, ΔE^{QM}, and f^{QM} are the standard deviation of the energy, the activation energy, and the number of degree of freedom of the active part, respectively. The static and dynamical effects of the environment are reflected through the energy barrier ΔE^{QM} and the standard deviation of the energy σ_E^{QM} of the active part. This modified RRK theory is referred to as the Matsubara-RRK (M-RRK) theory.

As mentioned earlier, it was pointed out by the ONIOM-MD method that the coordinated H_2 molecule rotates on the Pt atom in the $PtH(H_2)[P(t\text{-}Bu)_3]_2^+$ complex. It would be quite reasonable to apply the M-RRK theory to this behavior of the H_2 because the fluctuations in the energy of the active part become the energy source to overcome the energy barrier of the H_2 rotation. Unlike the conventional RRK theory, the M-RRK theory can give an insight into the dynamic behavior of the molecule, taking account of the dynamical environmental effects through the energy fluctuations. We calculated the ratio of the probability of the H_2 rotation of the different systems, a and b, as follows.

$$\frac{P_{\mathrm{a}}}{P_{\mathrm{b}}} = \frac{\left(1 - \dfrac{\Delta E_{\mathrm{a}}^{\mathrm{QM}}}{2\sigma_{E\mathrm{a}}^{\mathrm{QM}}}\right)^{f_{\mathrm{a}}^{\mathrm{QM}}-1}}{\left(1 - \dfrac{\Delta E_{\mathrm{b}}^{\mathrm{QM}}}{2\sigma_{E\mathrm{b}}^{\mathrm{QM}}}\right)^{f_{\mathrm{b}}^{\mathrm{QM}}-1}} \tag{18}$$

Here, the rotation energies of the H_2 at the various levels presented in Table 1 were used as the energy barriers ΔE^{QM}. As σ_E^{QM}, the standard deviation of the inner layer (active part) at the HF/BSI level presented in Table 7, was used. The number of degrees of freedom of the active part f^{QM} is 30 for R = H and 12 for R = Me and t-Bu. As shown in Table 8, the probability of the H_2 rotation is about 7 times larger for R = t-Bu than for R = Me at the HF/BSI level because the energy fluctuations $2\sigma_{E\mathrm{b}}^{\mathrm{QM}}$ is 1.7 times larger for R = t-Bu due to the large dynamical environmental effects. On the other hand, in the case of R = H without the dynamical environmental effects, the probability of the H_2 rotation is much reduced compared to the case of R = Me and t-Bu. These tendencies do not change in the other calculation levels.

If we do not consider the dynamical environmental effects in the active part, the energy fluctuations of the active part are in principle calculated as follows.[12]

$$\sigma_E^{\mathrm{QM,theorem}} = RT\sqrt{\frac{f^{\mathrm{QM}}}{2}} \tag{19}$$

Here, R is the gas constant. The probability of the H_2 rotation without the dynamical environmental effects is thence calculated as

$$P = \left(1 - \frac{\Delta E^{\mathrm{QM}}}{2\sigma_E^{\mathrm{QM,theorem}}}\right)^{f^{\mathrm{QM}}-1} \tag{20}$$

As shown in Table 8, it is obvious that the probability is significantly reduced without the dynamical environmental effects. For example, in the case of R = t-Bu, it is reduced to about one twenty-fourth. In the case of R = H, the probability increases when we use $\sigma_E^{\mathrm{QM,theorem}}$ calculated by eq 19, because the theoretical energy fluctuation $\sigma_E^{\mathrm{QM,theorem}}$ is larger than that obtained from the MD simulation. Matsubara's eq 1 also gives a similar tendency in the reactivity of the H_2 rotation, which increases in the order t-Bu > Me > H.

3.6. Evaluation of the Reactivity of the H_2 Dissociation from $PtH(H)_2(PR_3)_2^+$ (R = H, Me, and t-Bu) by Matsubara's Equation. Matsubara's eq 1 shows that the reaction becomes more facile when the magnitude of the energy fluctuations of the active part is enlarged by the dynamical effects of the environment. The dynamical environmental effects are the driving force of the reaction. Using Matsubara's equation, we examined the reactivity of the H_2 dissociation from the $PtH(H)_2(PR_3)_2^+$ (R = H, Me, and t-Bu) complexes, taking account of the dynamical environmental effects. The average potential energies and standard deviation of the potential energies of $PtH(H_2)(PR_3)_2^+$ at 200 K is presented in Table 7. The average energies are quite similar to those calculated by eq 21 according to the principle of equipartition of energy (see Table S1, Supporting Information) because the potential energy is enhanced by the kinetic energy.

$$\langle E \rangle = \frac{1}{2} fRT \tag{21}$$

The standard deviation of the QM potential energy of the inner layer increases in the order, t-Bu > Me > H, with the increase in the dynamical environmental effects. It was shown by eq 22[12] that the temperature of the inner layer rises to 411 K in the case of R = t-Bu.

$$T = \sqrt{\frac{2}{f^{\mathrm{QM}}}}\frac{\sigma_E^{\mathrm{QM}}}{R} \tag{22}$$

The magnitude of the oscillation of the QM potential energy also increases in the same order as shown in Table S2, Supporting Information. We used the E(gap) presented in Table S2 as the energy fluctuation σ_E^{QM} of Matsubara's equation because the energy obtained from the standard deviation cannot exceed the energy required for the H_2 dissociation. The change

TABLE 7: Average and Standard Deviation of the Potential Energies (kcal/mol) of $PtH(H_2)(PR_3)_2^+$ in the QM(HF/BSI)-MD (R = H) and ONIOM(HF/BSI:MM3)-MD (R = Me and t-Bu) Simulations at 200 K[a]

	E(QM,inner)			*E*(MM,outer)		*E*(ONIOM,entire)	
R	average	standard deviation	relative average energy[b]	average	standard deviation	average	standard deviation
Run 1[c]							
H	4.2	0.7	0.0				
Me	4.1	1.2	1.7	12.1	1.9	16.2	2.0
t-Bu	3.2	2.1	8.1	45.7	3.8	48.9	3.4
Run 2							
H	3.9	0.6	0.0				
Me	4.3	1.2	2.2	11.6	2.0	16.0	2.2
t-Bu	3.3	2.0	8.4	45.7	3.7	49.0	3.5
Run 3							
H	4.0	0.7	0.0				
Me	4.6	1.2	2.4	11.5	1.9	16.1	2.1
t-Bu	3.3	1.9	8.4	45.7	3.7	49.0	3.5

[a] The average energy is relative to the energy at 0 K (the energy of the optimized structure) for each R = H, Me, and t-Bu. [b] The relative average energy is the average energy relative to the average energy for R = H. [c] For R = t-Bu, the data collected from 5 to 40 ps were used, because the H_2 dissociated at 41.9 ps.

TABLE 8: Probability and Its Ratio and the Ratio of the Rate Constant of the H_2 Rotation of $PtH(H_2)(PR_3)_2^+$ (R = H, Me, and t-Bu) Calculated by Eqs *17* and *20* of the Matsubara-RRK Theory and Matsubara's Equation 1 at 200 K[a]

	eq *17*		eq *20*		eq *1*
R	probability	ratio	probability	ratio	ratio
HF/BSI					
H	2.13×10^{-11}	2.48×10^{-10}	1.24×10^{-4}	3.42×10^{-2}	3.18×10^{-2}
Me	1.15×10^{-2}	1.34×10^{-1}	3.62×10^{-3}	1.00	5.20×10^{-1}
t-Bu	8.58×10^{-2}	1.00	3.62×10^{-3}	1.00	1.00
HF/BSII					
H	2.72×10^{-6}	1.18×10^{-5}	5.05×10^{-3}	1.19×10^{-1}	1.16×10^{-1}
Me	7.65×10^{-2}	3.32×10^{-1}	4.22×10^{-2}	1.00	6.64×10^{-1}
t-Bu	2.30×10^{-1}	1.00	4.22×10^{-2}	1.00	1.00
B3LYP/BSII					
H	3.10×10^{-25}	1.57×10^{-23}	3.68×10^{-7}	8.78×10^{-3}	5.68×10^{-3}
Me	4.88×10^{-4}	2.46×10^{-2}	4.19×10^{-5}	1.00	3.75×10^{-1}
t-Bu	1.97×10^{-2}	1.00	4.19×10^{-5}	1.00	1.00

[a] The rotation energies of the H_2 at the various levels presented in Table 1 were used as the energy barrier ΔE^{QM} in eqs 17, 20, and 1.

in the potential energy for $PtH(H)_2[P(t\text{-}Bu)_3]_2^+$ (Figure S8, Supporting Information) also shows that the H_2 dissociation occurs when the potential energy of the inner layer reaches a maximum.

The ratio of the rate constant of the different systems, a and b, was calculated by Matsubara's equation as follows.

$$\frac{k_a}{k_b} = \frac{\exp\left(-\sqrt{\frac{f_a^{QM}}{2}}\frac{\Delta E_a^{QM}}{\sigma_{Ea}^{QM}}\right)}{\exp\left(-\sqrt{\frac{f_b^{QM}}{2}}\frac{\Delta E_b^{QM}}{\sigma_{Eb}^{QM}}\right)} \qquad (23)$$

Here, it is assumed that the frequency factors *A* for two different systems are the same. As shown in Table 9, by the replacement of t-Bu by the less bulky Me, the energy fluctuation σ_E^{QM} decreases by 2.1 kcal/mol at 200 K by the decrease in the dynamical environmental effects. On the other hand, the energy barrier increases only by 0.8 kcal/mol by the decrease in the static environmental effects. As a result, the rate constant of the H_2 dissociation is reduced to one-seventh because the change in the energy fluctuations is significantly reflected. This is in good agreement with the results of the ONIOM-MD simulations

TABLE 9: Ratio of the Rate Constant of the H_2 Dissociation of $PtH(H_2)(PR_3)_2^+$ (R = H, Me, and t-Bu) Calculated by Eq *23* of Matsubara's equation at 200 and 300 K

R	σ_E^{QM} (kcal/mol)[a]	ΔE^{QM} (kcal/mol)[b]	ratio
200 K			
H	2.45	10.2	9.41×10^{-4}
	2.45	8.9[c]	3.45×10^{-3}
	6.75[d]	10.2	6.23×10^{-1}
Me	4.65	9.7	1.52×10^{-1}
t-Bu	6.75	8.9	1.00
300 K			
Me	6.45	9.7	6.35×10^{-1}

[a] Half of *E*(gap) presented in Table S2 was used as the energy fluctuation σ_E^{QM}. [b] The interaction energies (INT) of the H_2 of $PtH(H_2)(PR_3)_2^+$ presented in Tables 1 and 2 were used as the energy barriers of the H_2 dissociation ΔE^{QM}. [c] ΔE^{QM} for R = t-Bu was used to artificially take account of the static environmental effects. [d] σ_E^{QM} for R = t-Bu was used to artificially take account of the dynamical environmental effects.

at 200 K that the H_2 dissociation takes place for R = t-Bu while not for R = Me. However, when the temperature is increased to 300 K, the rate constant increases to the similar value because the magnitude of the energy fluctuations for R = Me becomes nearly the same as that for R = t-Bu. This also coincides with

the ONIOM-MD simulations that the H_2 dissociation takes place even for R = Me at 300 K (Figure S7, Supporting Information).

In the case of R = H without the environmental effects, the rate constant is reduced to about one-thousandth compared to the case of R = t-Bu. When we take account of the static environmental effects by artificially decreasing the energy barrier ΔE^{QM}, the rate constant becomes only 4 times larger. On the other hand, when we take account of the dynamical environmental effects by artificially increasing the energy fluctuations σ_E^{QM}, the rate constant becomes 662 times larger. This shows that the dynamical environmental effects contribute much more to the reaction compared to the static environmental effects.

4. Concluding Remarks

The reactivity of the chemical reaction has been evaluated by the energy barrier obtained from the energy surface of the reaction. However, by this conventional manner, we cannot know how the reaction exceeds the energy barrier and what is the driving force of the reaction, which would be the next subjects to understand in the chemical reaction. In the present study, 'the energy fluctuations' afforded one of the clues to answer these questions. As we have recently discovered, the energy fluctuations are much more important factors than the energy barrier to determine the reactivity of the chemical reaction.

To evaluate the reactivity of the chemical reaction, the entire system has to be divided into the active part and the environment. This would become more important with the increase in the scale of the molecular system. The essential barrier of the chemical reaction exits in the active part. When the active part overcomes a barrier, the reaction proceeds. The increase in the magnitude of the energy fluctuations of the active part by the dynamical environmental effects, which corresponds to the increase in the temperature of the active part, facilitates the chemical reaction. The dynamical environmental effects are the significant driving force of the chemical reaction. Although the conventional static environmental effects affect the energy barrier, the dynamical environmental effects affect the energy fluctuations. Not the static effects but the dynamic effects of the environment are the dominant factors that determine the reactivity of the chemical reaction. These were indicated in this study for the reaction of the $PtH(H_2)[P(t\text{-}Bu)_3]_2^+$ complex.

We applied the ONIOM-molecular dynamics (MD) method to the $PtH(H_2)[P(t\text{-}Bu)_3]_2^+$ complex and examined the dynamical environmental effects of the substituents t-Bu of the ligands on the reactivity of the coordinated H_2 molecule. The ONIOM-MD simulations showed that the dynamical environmental effects of the t-Bu increase the magnitude of the energy fluctuations of the active part. Both rotation and the dissociation of the coordinated H_2 molecule are significantly promoted by the increase in the magnitude of the energy fluctuations of the active part. These were verified by the Matsubara-RRK (M-RRK) theory proposed in this study and Matsubara's equation. Thus, it was found that the dynamical environmental effects, which affect the energy fluctuations of the active part, are dominant factors to determine the reactivity of the coordinated H_2 molecule. The reactivity of the chemical reaction would be predicted with a higher accuracy by considering the dynamical environmental effects through the energy fluctuations as new factors.

Acknowledgment. This study was supported in part by grants from the Ministry of Education, Culture, Sports, Science and Technology of Japan.

Supporting Information Available: Figures S1−S8 and Tables S1 and S2. This material is available free of charge via the Internet at http://pubs.acs.org.

References and Notes

(1) Maseras, F.; Morokuma, K. *J. Comput. Chem.* **1995**, *16*, 1170–1179.
(2) Matsubara, T.; Sieber, S.; Morokuma, K. *Int. J. Quantum Chem.* **1996**, *60*, 1101–1109.
(3) Matsubara, T.; Maseras, F.; Koga, N.; Morokuma, K. *J. Phys. Chem.* **1996**, *100*, 2573–2580.
(4) Svensson, M.; Humbel, S.; Froese, R. D. J.; Matsubara, T.; Sieber, S.; Morokuma, K. *J. Phys. Chem.* **1996**, *100*, 19357–19363.
(5) Dapprich, S.; Komáromi, I.; Byun, K. S.; Morokuma, K.; Frisch, M. J. *J. Mol. Struct. (THEOCHEM)* **1999**, *461−462*, 1–21.
(6) Vreven, T.; Morokuma, K. *J. Comput. Chem.* **2000**, *21*, 1419–1432.
(7) Morokuma, K. *Bull. Korean Chem. Soc.* **2003**, *24*, 797–801.
(8) Frisch, M. J.; Trucks, G. W.; Schlegel, H. B.; Scuseria, G. E.; Robb, M. A.; Cheeseman, J. R.; Montgomery, Jr., J. A.; Vreven, T.; Kudin, K. N.; Burant, J. C.; Millam, J. M.; Iyengar, S. S.; Tomasi, J.; Barone, V.; Mennucci, B.; Cossi, M.; Scalmani, G.; Rega, N.; Petersson, G. A.; Nakatsuji, H.; Hada, M.; Ehara, M.; Toyota, K.; Fukuda, R.; Hasegawa, J.; Ishida, M.; Nakajima, T.; Honda, Y.; Kitao, O.; Nakai, H.; Klene, M.; Li, X.; Knox, J. E.; Hratchian, H. P.; Cross, J. B.; Bakken, V.; Adamo, C.; Jaramillo, J.; Gomperts, R.; Stratmann, R. E.; Yazyev, O.; Austin, A. J.; Cammi, R.; Pomelli, C.; Ochterski, J. W.; Ayala, P. Y.; Morokuma, K.; Voth, G. A.; Salvador, P.; Dannenberg, J. J.; Zakrzewski, V. G.; Dapprich, S.; Daniels, A. D.; Strain, M. C.; Farkas, O.; Malick, D. K.; Rabuck, A. D.; Raghavachari, K.; Foresman, J. B.; Ortiz, J. V.; Cui, Q.; Baboul, A. G.; Clifford, S.; Cioslowski, J.; Stefanov, B. B.; Liu, G.; Liashenko, A.; Piskorz, P.; Komaromi, I.; Martin, R. L.; Fox, D. J.; Keith, T.; Al-Laham, M. A.; Peng, C. Y.; Nanayakkara, A.; Challacombe, M.; Gill, P. M. W.; Johnson, B.; Chen, W.; Wong, M. W.; Gonzalez, C.; Pople, J. A. Gaussian 03; Gaussian, Inc., Wallingford, CT, 2004.
(9) Matsubara, T.; Dupuis, M.; Aida, M. *Chem. Phys. Lett.* **2007**, *437*, 138–142.
(10) Matsubara, T.; Dupuis, M.; Aida, M. *J. Phys. Chem. B* **2007**, *111*, 9965–9974.
(11) Matsubara, T.; Dupuis, M.; Aida, M. *J. Comput. Chem.* **2008**, *29*, 458–465.
(12) Matsubara, T. *J. Phys. Chem. A* **2008**, *112*, 9886–9894.
(13) Gusev, D. G.; Notheis, J. U.; Rambo, J. R.; Hauger, B. E.; Eisenstein, O.; Caulton, K. G. *J. Am. Chem. Soc.* **1994**, *116*, 7409–7410.
(14) For example, see:(a) Esteruelas, M. A.; Oro, L. A. *Chem. Rev.* **1998**, *98*, 577–588.
(15) Hay, P. J.; Wadt, W. R. *J. Chem. Phys.* **1985**, *82*, 299.
(16) Rappe, A. K.; Casewit, C. J.; Colwell, K. S.; Goddard, W. A., III; Skiff, W. M. *J. Am. Chem. Soc.* **1992**, *114*, 10024.
(17) Dupuis, M.; Marquez, A.; Davidson, E. R. HONDO 2001, based on HONDO 95.3, available from the Quantum Chemistry Program Exchange (QCPE), Indiana University.
(18) Beeman, D. *J. Comp. Phys.* **1976**, *20*, 130–139.
(19) Berendsen, H. J. C.; Postma, J. P. M.; van Gunsteren, W. F.; DiNola, A.; Haak, J. R. *J. Chem. Phys.* **1984**, *81*, 3684–3690.
(20) Lee, C.; Yang, W.; Parr, R. G. *Phys. Rev. B* **1988**, *37*, 785–789.
(21) Becke, D. *J. Chem. Phys.* **1993**, *98*, 5648–5652.
(22) (a) Kubas, G. J.; Burns, C. J.; Eckert, J.; Johnson, S. W.; Larson, A. C.; Vergamini, P. J.; Unkefer, C. J.; Khalsa, G. R. K.; Jackson, S. A.; Eisenstein, O. *J. Am. Chem. Soc.* **1993**, *115*, 569–581. (b) Eckert, J.; Kubas, G. J.; Hall, J. H.; Hay, P. J.; Boyle, C. M. *J. Am. Chem. Soc.* **1990**, *112*, 2324–2332. (c) Eckert, J.; Kubas, G. J. *J. Phys. Chem.* **1993**, *97*, 2378–2384. (d) Eckert, J.; Jensen, C. M.; Jones, G.; Clot, E.; Eisenstein, O. *J. Am. Chem. Soc.* **1993**, *115*, 11056–11057. (e) Eckert, J.; Kubas, G. J.; White, R. P. *Inorg. Chem.* **1992**, *31*, 1550–1551. (f) Eckert, J.; Albinati, A.; White, R. P.; Bianchini, C.; Peruzzini, M. *Inorg. Chem.* **1992**, *31*, 4241–4244.
(23) (a) Jalon, F. A.; Otero, A.; Manzano, B. R.; Villasenor, E.; Chaudret, B. *J. Am. Chem. Soc.* **1995**, *117*, 10123–10124. (b) Antinolo, A.; Carrillo-Hermosilla, F.; Fajardo, M.; Garcia-Yuste, S.; Otero, A.; Camanyes, S.; Maseras, F.; Moreno, M.; Lledos, A.; Lluch, J. M. *J. Am. Chem. Soc.* **1997**, *119*, 6107–6114. (c) Barrio, P.; Esteruelas, M. A.; Lledos, A.; Onate, E.; Tomas, J. *Organometallics* **2004**, *23*, 3008–3015.

JP810336U